Specimen preparation for "block face" scanning electron microscopy (BFSEM). An energy-dispersive X-ray spectroscopy study

M. Teresa Núñez-López[1], Gilberto del Rosario-Hernández[2], Laura López-Gómez[3], Pedro Mestres-Ventura[4]

[1]*Facility for Electron Microscopy (CAT), Medical Faculty, University Rey Juan Carlos, 28922 Alcorcon, Madrid (Spain),* [2]*Laboratory for Electron Microscopy, Centre for Technical Support (CAT), University Rey Juan Carlos, 28933 Mostoles, Madrid (Spain),* [3]*Department of Human Histology and Pathology, Faculty for Health Sciences, University Rey Juan Carlos, Av. de Atenas s/n, 28922 Alcorcon, Madrid (Spain),* [4]*Department of Anatomy and Cell Biology, Medical School, Saarland University, 66421 Homburg (Germany)*

SUMMARY

In this paper we describe a SEM block-face technique in which block faces of large dimensions can be examined in a high-resolution SEM under high vacuum. The results of different tissue contrast methods have been studied and, in addition to osmium, potassium permanganate has been used as a staining medium for the first time in BFSEM. The study also examined the effects of uranyl acetate and phosphotungstic acid. The following organs of adult albino rats were examined: colonic mucosa, spinal ganglion, anterior pituitary gland and exocrine pancreas.

Six preparation protocols, referred to here as treatments, were applied and evaluated according to three criteria: 1st the visual quality of the digital images, 2nd the measurements of the signal-noise ratio (SNR) of the digital images with and without beam deceleration (BD), and 3rd the X-ray microanalysis of samples, treated according to the 6 proposed protocols, demonstrating the presence and relative quantity of the elements used to stain the cellular structures, enabling visualisation with the electron microscope.

In conclusion, it can be said that treatments with osmium produced better results than those containing potassium permanganate. Treatments with the addition of thiocarbohydrazide (TCH) considerably increased the osmium deposits (ligand effect) and proved highly effective.

Finally, it should be noted that the method proposed, called here 2D BFSEM, can be very useful not only in histology but also in histo-pathology, for example in the study of biopsies and - last but not least - in embryology: all these are situations in which it is important to avoid a loss of material due to preparation exigencies.

Key words: Block face – BFSEM – Tissue preparation – EDX – Electron microscopy

INTRODUCTION

The term "block face" refers to the surface of the embedding block, which has been generated after cutting with a microtome. The approach of examining the block surface was first published in the 1940s by Hegre and Brashear (1946). These authors had the ingenious idea of taking embryos, impregnating them with lead salts and then embedding them in paraffin. The lead salts were stained dark by means of a sulfur-containing solution applied to the surface of the block. With this treatment the structure of the embryo could be made visible on the surface of the block with astonishing clarity. Sections were produced and, after each cut, the surface of the embedding block

Corresponding author: María Teresa Núñez López, PhD. Laboratory for Electron Microscopy of the Medical Faculty, Centre for Technical Support (CAT), University Rey Juan Carlos, Av. de Atenas s/n, 28922 Alcorcón, Madrid, Spain. Phone: +34 914 888 645. E-Mail: teresa.nunez@urjc.es

was photographed to make a photo series and assembled into a film (Hegre and Brashear, 1947). In other words, if, instead of examining the sections, we wish to microscopically examine the surface of the block, the so-called block-face, then this can only be achieved with falling electrons or photons. This is possible with the confocal-laser-scanning microscope (CLSM), where images of serial optical sections can be obtained and processed to 3D-reconstructions (Bajcsy et al., 2006; Wanninger, 2007).

This technique was introduced in scanning electron microscopy by Leighton (1981), who thus created the block face SEM method (BFSEM) to produce 3D reconstructions of cells and tissues. This author proposed this procedure to circumvent many problems which are closely associated with obtaining serial thin sections for TEM (compression, deformation, loss of single thin sections, etc.); problems which have a great influence on the shape and size of cellular structures, and therefore are relevant parameters when trying to perform tri-dimensional reconstruction of cellular and tissue ultrastructure. To obtain a series of images of the block-face, an ultra-microtome was installed inside the specimen chamber of the SEM. The sections were discarded, but the surface of the block on which they were made was prepared for examination in SEM (Leighton, 1981, Denk and Horstmann, 2004). In the images obtained with backscattered electrons (BSE), the gray colors were inverted, resulting in images which are hardly distinguishable from those obtained from thin sections with a TEM, an approach which greatly simplifies the interpretation of the block-face pictures.

Although Leighton had demonstrated the feasibility of the technique, more than a decade passed before the technology reached maturity. New SEM devices, better ultra-microtomes inside the SEM, and special software to control the devices and to manage the reconstructions had to be developed (Denk and Horstmann, 2004, see also www.gatan.com).

The development of the environmental scanning electron microscope (ESEM, Danilatos, 1988, 1994) in the nineties of the last century opened new possibilities for the technology Leighton had designed. The fact that non-coated samples could be examined in an SEM even if they were not per se conductive, paved the way for automation of the block face technique (Denk and Horstmann, 2004). Automation of the work with the ultra-microtome inside the microscope, location of the coating system in the specimen chamber as well as the highly reliable acquisition of image series and, finally, their subsequent processing to produce precise 3D reconstructions, have become possible not only through advances in mechanics and electronics, but also through the development of a corresponding software (Denk and Hortstmann, 2004; Titze and Denk, 2013; Titze and Genoud, 2016).

Recently ion beam scanning electron microscopy (FIB-SEM, a procedure associated with cryo-EM methods) has been used in order to examine the architecture of tissues, thus enlarging the range of possible procedures in volume electron microscopy (Bushby et al., 2011; Schertel et al., 2013).

Along with the instruments used, specimen preparation plays a crucial role in the procedure as optimal contrast effects are vital for high-quality imaging. In SEM the primary electron beam is directed at the specimen, resulting in secondary (SE) and backscattered electrons (BSE), providing varying informational content (Ogura and Hasegawa, 1980; Peters, 1985). While the SEs provide a precise image of the surface of the sample, the BSEs give in-depth information about the material and its composition (atomic number), which is important in our context. Thus, with BSE, heavy metals (staining) present in the sample can be identified, as they are an important source of this type of electrons in SEM (Bloom and Goodpasture, 1976; Thiebaut et al., 1986, Mestres et al., 1988). This means that, if the surface of the resin block with tissue stained with the heavy metal solutions commonly used in TEM is examined in a SEM, images of the cell structures can be primarily obtained with the BSE signal (Laue et al., 2005).

Leighton already used the standard staining protocol for transmission electron microscopy, i.e. chemical fixation, staining with osmium tetroxide and embedding in epoxy resin. Essentially this procedure is still in place although strategies to intensify the deposit of heavy metals in the samples are being increasingly implemented as this considerably improves the quality of the images (Seligman et al., 1966; Malick et al., 1975; in connection with BFSEM see Deerinck et al., 2010; Mikula et al., 2012). However, the relative or absolute amounts of the metallic atoms deposited in the sample after staining is currently unknown an estimation can only be based on the visualized contrast effects.

The BFSEM technique described here is less spectacular but could nevertheless prove useful if applied to large-size specimens, enabling the study of the ultrastructure of cells and tissues, with the obvious advantages over the standard TEM procedure.

Standard TEM requires the trimming of the embedded material to a size suitable for the preparation of thin sections. This entails a considerable reduction in block size which could result in substantial material loss. In the past this handicap could only be partially compensated for by the use of special trimming techniques such as the "mesa pyramid" principle (Heimer, 1970). This problem can be avoided in BFSEM as it permits the examination of large areas (block face side of 1 cm or more). In our procedure the resin block is trimmed in the form of a pyramid, leaving a smooth area (block face) on the tip, from which semi-thin sections can be obtained. Once dyed, these can be studied with the light microscope; a practicable form of correlative EM-LM microscopy. Afterwards, the block face is covered with a thin coating of carbon, or even platinum, to ensure conductivity, and finally the block is placed into the SEM and exam-

ined.

In the present study, two main aspects are at the forefront: 1) the elementary analysis of contrast-giving elements to tissues, as well as their influence on the images, and 2) the performance of a two-dimensional BFSEM microscopy (2D-BFSEM) under high vacuum, demonstrating, though with certain limitations, the practicability of block face in an HRSEM. For these purposes, organs of adult albino rats such as the colon, spinal ganglion, anterior lobe of pituitary gland and exocrine pancreas were prepared for micro-analytical and structural studies.

MATERIALS AND METHODS

In the present study, adult rats of both sexes (Wistar, 250 g BW) were used. They were kept under the conditions stipulated by the EU for animal experimentation. An authorization from the Ethics Commission of the University Rey Juan Carlos has been issued. The animals were euthanized by asphyxiation with carbon dioxide, a method approved by the American Veterinary Association.

The colon was removed, washed with a physiological saline solution, partitioned into small segments and fixed by immersion in 2.5% glutaraldehyde at pH 7.4 buffered with Na-cacodylate 0.12 M. Thereafter it was post-fixed in buffered osmium tetroxide 2%, dehydrated in an ascending ethanol series and embedded in epoxy resin (TAAB embedding kit or Science Services EMBed-812 embedding kit) and polymerized at 60ºC (Mestres et al., 2014).

Tissue samples already fixed with glutaraldehyde were treated with contrast-giving compounds and the following protocols, which had proved themselves in previous studies, were applied (see Table 1).

For histological applications of 2D-BFSEM, a second group of animals was intravascularly perfused with a solution containing 2.5% glutaraldehyde and buffered with 0.12 M cacodylate at pH 7.4 (Fluka) under anesthesia (Ketamine 90 mg/Kg BW and Medetomidine 0.25 mg/Kg BW).

The following organs were collected: trigeminal ganglion, pituitary anterior lobe and pancreas. These organs were dissected under a stereomicroscope and divided into small pieces of approximately 4 mm side length and 1-2 mm thick. These samples were post-fixed for 2 hours at +8ºC in the same glutaraldehyde solution as used for vascular perfusion, then treated in accordance with treatment 2 (Table 1) and dehydrated and embedded as described above.

The block face was prepared first by trimming the resin block with a glass knife, leaving at the tip a square or block face of several mm side length, and then the face of the block itself was smoothened with a diamond histo-knife (Diatome).

Thick sections (1 µm) were made for histological orientation and stained with methylene blue (Richardson et al., 1960). Thin sections (90 nm)

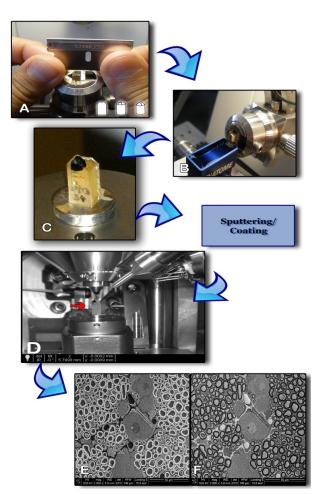**Fig 1.** Flow diagram for BFSEM tissue preparation. **A**) Trimming, **B**) Smoothing of the block surface, **C**) Assembly of the resin block on the aluminum stub, **D**) Location of the object in the microscope chamber, **E**) BSE image of a detail of the block (spinal ganglion), **F**) previous image inverted, with similarity to a TEM image.
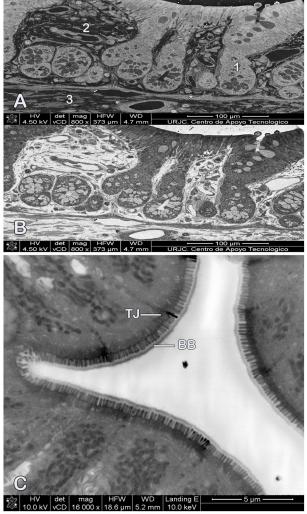
for correlative TEM were also prepared and stained with lead citrate (Reynolds, 1963). The thin sections were examined in a Jeol JEM 1010 equipped with a digital camera Mega View III (SIS, Münster/NRW, Germany).

The resin blocks were then mounted on an aluminum stub and fixed with conductive adhesive. As the samples are not conductive, they had to be coated, one series of them with carbon (carbon layer thickness 6.3 to 11 nm) in an Electron Beam Evaporator vapor deposition system (AL-TEC MED 020 coupled to Leica EM EVM 030 & EK 030) and another series with platinum (layer thickness >4 nm) or gold (layer thickness 10-nm) in a sputter coater (BAL-TEC, SCD 005).

Images of the block face were obtained with a Nova Nano SEM 230 FEG (FEI) operating at 3-10 kV, equipped with a BSE detector [BSED=backscattered electron detector, low voltage high contrast solid state, vCD (FEI)], and an Everhart-Thornley type detector (ETD, FEI) for secondary electrons. The BSE pictures were then inverted, resembling standard TEM images in appearance (Fig. 1).

Table 1. Methods and literature

Treatment 1	Tannic ac. 2% followed by 2% OsO_4 buffered with cacodylate 0.12 M pH 7.4	Plattner and Zingsheim (1987)
Treatment 2	Solution of OsO_4 2% with potassium ferrocyanide 1.5% buffered with 0.12 M cacodylate pH 7.4, followed by thiocarbohydrazide (TCH) and OsO_4 2% again	Seligman et al. (1966) Geyer (1969) Glauert (1975)
Treatment 3	Solution of OsO_4 2% buffered with 0.12 M cacodylate pH 7.4, then $KMnO_4$ 1.5% in saline, followed by uranyl acetate 1% in acetone 25%	Brightman and Reese (1969) Geyer (1969) Luft (1971)
Treatment 4	$KMnO_4$ 1% in saline	Luft (1971)
Treatment 5	$KMnO_4$ followed by uranyl acetate as above	Luft (1971) Brightman and Reese (1969)
Treatment 6	$KMnO_4$ followed by 2% OsO4 as above and uranyl acetate and phospho-tungstic acid (PTA) 1% in acetone 70%	Geyer (1969)

Fig 2. Colonic mucosa. **A**) BSE image. 1: crypt, 2: *lamina propria*, 3: *muscularis mucosae*. **B**) Image A inverted. **C**) Apical pole of colonic enterocytes showing a well-developed brush border (BB). TJ: Tight junctions. Note a grey material over the microvilli corresponding to the glycocalyx.

The image quality was assessed by determining the signal-noise-ratio (SNR) (Peters, 1985; Thong et al., 2001). This parameter was measured using the software Image J and the results were expressed in decibels (dB). Pictures were taken with and without Beam Deceleration (BD) (Ohta et al., 2012).

Samples of rat colon treated according to the protocols listed in Table 1 were micro-analytically (EDX) examined. An epoxy resin block without any tissue served as a control. For microanalysis the samples were coated with carbon (layer thickness 12 nm) in an Electron Beam Evaporator (see above) and the measurements performed in an XL30 ESEM (FEI / Philips), equipped with an X-Ray (EDAX) detector with a SUTW-Sapphire window (super ultrathin window 0.3 μm thick). The measurements were performed at 20kV and under high vacuum. The EDX detector was placed at an angle of 35°. The data were acquired within 30 sec. without tilting the specimen stage. The spectra were processed with the EDX Control software version 3.34 (EDAX).

Taking as a reference the number of counts (net intensity, height of peaks), a statistical analysis was carried out to establish an average per element and region studied (n=6 points at least per average). This average corresponds to the concentration of each element at the point of measurement. EXCEL (version 2007) was used for the graphic representation of these data.
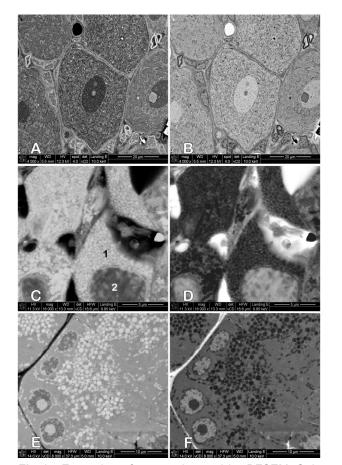
For orientation and selection of EDX measuring points, images of the surfaces were recorded with the BSE Robinson detector at 20 kV and 10 mm WD.

RESULTS

Morphology

Colon samples, processed according to the 6 treatments described, were coated with carbon or with platinum and examined in HRSEM under high vacuum, using BSE for imaging at several magnifications for comparative purposes and for structural studies. The grey values of the BSE images were inverted to create images similar to TEM pictures.

Fig. 2 depicts an example of this procedure. The histological outlines of the colon wall are easily recognizable at low magnifications and there are no significant differences between the 6 treatments. Differences between treatments were first detectable at higher magnifications, for instance, at 4000X and higher (Fig. 2). While treatments 1, 2 and 3 revealed the finest details of the cell and

Fig 3. Examples of organs imaged by BFSEM. Spinal ganglion. A (BSE image) and B (inverted image). 5 neurons can be seen. At the left small cell nuclei located between two neurons corresponding to glia cells. Some myelinated nerve fibers can easily recognized, as well as a blood capillary as a hole (upper part) due to vascular perfusion of the animal. Pituitary gland (anterior lobe). C (BSE image) and D (inverted image). Note the high number of secretory granules (1) and the characteristic appearance of the cell nucleus (2). Exocrine pancreas. E (BSE image) and F (inverted image). The image shows the basal part of an acinus with several cell nuclei and numerous zymogen granules

Table 2. Measurements of the signal noise ratio.

Treat-ments	BD*	800X Visual field 100%	4000X Visual field - 96,00%	16000X Visual field - 99,65%
1	no	10,82	12,67	14,07
1	yes	12,57	12,58	16,53
2	no	9,86	11,29	13,17
2	yes	11,49	15,86	14,59
3	no	12,19	11,29	13,91
3	yes	--------	19,14	11,57
4	no	18,35	9,16	8,84
4	yes	10,97	9,26	9,83
5	no	13,72	13,61	16,19
5	yes	10,36	13,90	9,64
6	no	9,38	10,83	10,48
6	yes	12,57	11,98	15,48

(*): BD= beam deceleration

nervous system, such as the cell body of neurons, with nucleus and nucleolus and a cytoplasm that is rich in organelles. The cell bodies of the neurons appear to be surrounded by thin sheets of ganglionic glia, satellite cells, permitting a view of the different cellular membranes of each of these formations (Fig. 3A and B). Myelinated axons are also observed with a dark myelin sheath. Components of the stroma containing blood capillaries are also present (Fig. 3A and B).
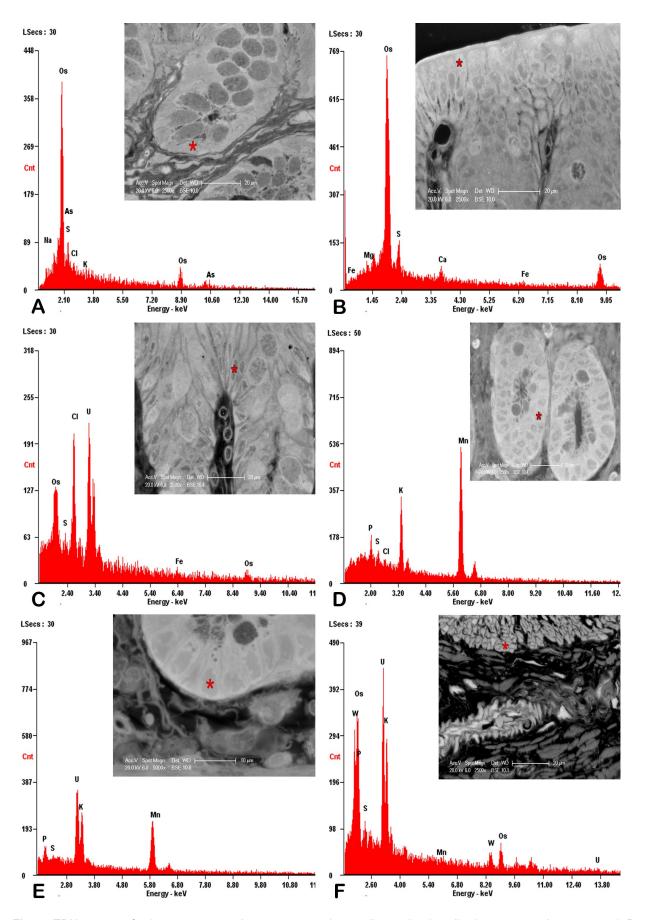
Another example of the effectiveness of these methods is the anterior pituitary, an endocrine gland constituted of hormone-secreting cells, and as such rich in secretory granules of different sizes depending on the cell type, i.e., with a different hormone content (Fig. 2C and D).

In the exocrine pancreas the secretory granules are well identified, as are cytological details such as cell nuclei located in the basal region of the cell. The granules occupy a supra-nuclear or apical position (Fig. 3E and F). In the block-face SEM images, nucleus and chromatin patterns, as well as the nucleolus, correspond very much with those seen in standard TEM pictures (Fig. 3E and F).

Image quality

Image quality was determined calculating the signal/noise ratio (SNR). For this purpose, colon images with comparable histological motifs were selected. The images were obtained with and without the application of beam deceleration (BD) and, as already mentioned in the Material and Methods section, the working conditions of the microscope were not changed when using BD.

In the images of samples handled according to treatment 1, the SNR increased slightly with an increase in image magnification. Taking the SNR of images at 800X as a reference, the value of the SNR increased in the next higher magnifications by 15%, to reach 30% at 16000X (Table 2). With BD application the SNR value increased by 16%

tissue structure, treatments 4, 5 and 6 yielded less satisfactory results. In these latter cases the subcellular details were less evident as there are hardly any differences in contrast in the background and cellular structures (not shown).

In the images of the wall of the colon fixed according to method 2, cytological details such as tight junctions can be recognized, as well as the brush border with its glycocalyx, closely associated with the microvilli (Fig. 2C). In the apical cytoplasm in the figure, one can see dense mitochondria that appear to be more or less grouped (Fig. 2C). The cell membrane is also clearly visible on the lateral surface between neighboring enterocytes (Fig. 2C).

The examination of other organs confirmed the good performance of both method 2 and method 3. For instance, in block-face SEM images of the spinal ganglion one can appreciate all the ultrastructural details of this organ of the peripheral

Fig 4. EDX-spectra of colon mucosa specimens processed according to the described treatments. A: treatment 1, B: treatment 2, C: treatment 3, D: treatment 4, E: treatment 5, F: treatment 6. The inserts show the location of the sites where measurements were performed (red asterisk).

and this value remained unchanged in higher magnifications. However, there was a slight increase in SNR at 16000X (Table 2).

In the case of treatment 2, SNR increased up to 33.6% when compared with the values measured at 800X and without BD (Table 2). With BD application there was an increase in SNR of between 27.00% and 38.00% (Table 2).

In treatment 3, the SNR value compared with the values measured at 800X and without BD and then rose by to 14.1%. This increase of SNR was even more pronounced when BD was applied, reaching values of 83.5% higher than those measured at the same magnification without BD. However, increases of SNR at higher magnifications were not observed (Table 2).

In treatment 4, and in contrast with the previous treatments, SNR diminished with increasing magnifications.

In treatment 5, the SNR values differed slightly from those measured in specimens handled according to treatment 4. A comparison of SNR at 800X and at 16000X showed an increase of 18%. These samples did not display any effect of BD on SNR (Table 2).

Finally, in treatment 6, and comparing SNR values at 800X and 16.000X, an increase of 11% in this parameter was registered (Table 2). Using BD, the values of SNR at 800X were 34% better with an increase of up to 47.75 % at magnifications to the order of 16000X. At lower magnifications (2000 and 4000X) the SNR value increased by 5% to 10.6% and BD did not seem to have had any effect (Table 2).

X-Ray microanalysis

For microanalysis (point measurements) predetermined locations in the tissue were selected, such as the cytoplasm of enterocytes, the cell nucleus of these cells, smooth muscle cells of the *muscularis mucosae* layer and areas of the connective tissue of the mucosa, where bundles of collagen fibers were clearly identified.

In the specimens processed according to treatment 1, the spectra were characterized by two peaks of osmium, corresponding to the lines M and L of this element (Figure 4 A). In addition, a peak of arsenic was also detected, which was almost certainly related to the buffer cacodylate used in the fixative solutions (Fig. 4A). Other elements were related to the tissue itself and with the solutions used in the preparation of the tissue appearing in the spectrum of the corresponding treatment (Fig. 4A).

In the spectra of specimens processed according to treatment 2, a prominent osmium peak represented by the line M, and another peak corresponding to the line L of this element were observed (Fig. 4B). Both peaks indicate the presence of a high amount of this element (Fig. 4B). The peak corresponding to sulfur (line K) is directly related to TCH, a molecule that contains that element (Fig. 4B). Finally, the iron peak (line K) that appears in these spectra is related to the potassi-

um ferrocyanide, which is present in the fixing solution used in this treatment (Fig. 4B).

In treatment 3, the fixing solution is again applied according to Karnovsky with potassium ferrocyanide, followed by a step of uranyl acetate. In the spectrum the peak of uranium (line M) which appeared is higher than the osmium peak (Fig. 4C). It is remarkable that, in this case, the osmium peak is 61.00 % lower than in treatment 2 and over 40% lower than in treatment 1.

In treatment 4, potassium permanganate was used instead of osmium tetroxide. The spectrum here shows the corresponding peaks for manganese (line K) and potassium (line K) (Fig. 4D).

Treatment 5 differs from the previous one in that uranyl acetate was added to the specimen. In the spectra, a uranium peak (line M) of considerable height is displayed (Fig. 4E). In contrast, the manganese peak is lower than in treatment 4 (Fig. 4E).

Treatment 6 followed the same protocol as treatment *5, but* with additional steps with osmium tetroxide and phosphotungstic acid. In this treatment it is remarkable that the uranium peak is higher than in treatment 5 (Fig. 4F). In contrast, the peak for manganese is rather low compared with those in the spectra of treatment 4 and 5. In the spectrum, two peaks of tungsten corresponding to its lines M alpha and L alpha can be distinguished (Fig. 4F). With regard to osmium, it is noteworthy that the peaks are similar to others, for example those seen in treatment 1.

A graphical representation of the net intensities of the peaks provides a clearer expression of the differences in concentration of the elements mentioned above (Tables 3 and 4). As the concentration of these elements depends on the histological location of the measurement point, a differentiation is made between measurements in the cellular cytoplasm and those in the loose connective tissue - particularly in areas with fibers and without cells. As previously mentioned, the microanalytic analysis in treatments 4, 5 and 6 shows differences in the concentration of uranium and manganese. In the presence of uranyl acetate, the concentration of manganese from potassium permanganate present in the tissue decreases at the same time as that of uranium increases considerably, a process that seems to be enhanced in the presence of osmium tetroxide and phosphotungstic acid.

DISCUSSION

In the present study a 2D block-face modus for SEM has been described, which differs in many respects from that conceived and developed by the group of Winfried Denk in Heidelberg and called 3D serial BFSEM (SBFSEM).

These differences can be summarized as follows. Firstly, this is not a modus designed for 3D studies: its main advantage is that it enables the examination of block faces of large dimensions, which could be very useful in histology, embryology and also in histo-pathology. Secondly, it can be performed in a conventional SEM at high vacuum,
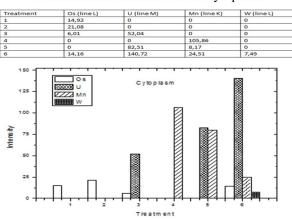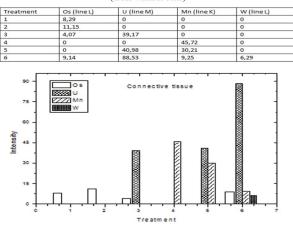
TABLE 3

Net Intensities measured in the cytoplasm

Treatment	Os (line L)	U (line M)	Mn (line K)	W (line L)
1	14,92	0	0	0
2	21,08	0	0	0
3	6,01	52,04	0	0
4	0	0	105,86	0
5	0	82,51	8,17	0
6	14,16	140,72	24,51	7,49

TABLE 4

Net Intensities measured in the connective tissue

(areas without cells)

Treatment	Os (line L)	U (line M)	Mn (line K)	W (line L)
1	8,29	0	0	0
2	11,15	0	0	0
3	4,07	39,17	0	0
4	0	0	45,72	0
5	0	40,98	30,21	0
6	9,14	88,53	9,25	6,29

requiring albeit a conducting coating, in contrast with other investigations in which BFSEM is performed under environmental conditions (Denk and Horstmann, 2004; Laue et al., 2005). Thirdly, the sectioning of the block and the preparation of the block faces takes place outside of the microscope using a conventional ultra-microtome: this circumstance represents a main difference to the SBF-SEM, in which a special microtome operates within the specimen chamber of the SEM (Leighton 1981; Denk and Horstmann, 2004).

Nevertheless, the BFSEM modus presented here retains some points in common with the original block-face procedure. As in SBFSEM, the signal used to produce images is BSE, and, for further studies, the grey values of the pictures are inverted, thereafter resembling TEM images (Crewe and Lin, 1976; Carter, 1980; Seiter et al., 2014).

Our experience and that of other authors is that an important property of the face of the block is its smoothness; topographic irregularities especially impair the digital images. We used the traditional

diamond knife; the surface of the block is dependent on the quality of its edge. However, in the last few years, alternative techniques such as *focused ion-beam-milling* (FIM) have emerged, which have a great potential to produce surfaces with molecular perfection, thus largely avoiding disturbances on the surface (Knott et al., 2008; Schertel et al., 2013).

For SBFSEM the specimens are stained with solutions of heavy metal salts – those traditionally used in transmission electron microscopy (Geyer, 1969). In addition to the classical osmium tetroxide (Porter et al., 1945; Palade, 1952), the present study applied potassium permanganate several times, a chemical introduced in electron microscopy by Robertson (1958, 1981) and still in use (Inoue, 1995), but not as yet used in SBFSEM. Other contrast-giving heavy metals such as uranium, tungsten and iron have been used in our protocols, as they are already well-established in transmission and also in scanning electron microscopy, as, here, they make the specimens conductive (Glauert, 1975; Plattner and Zingsheim, 1987). Although not been applied in our study, lead aspartate should also be mentioned; recently introduced as additional *en bloc* staining for BFSEM (Deerinck et al., 2010).

In order to evaluate the results obtained, three approaches were followed: first the degree of preservation of the cellular ultrastructure was examined; second, the signal/noise ratio of the digital pictures was measured, and thirdly, X-ray microanalysis of the specimens was carried out to detect and quantify the contrast- giving elements.

Both osmium tetroxide and potassium permanganate have a high affinity for structures rich in phospholipids, such as cyto-membranes (Bozzola et al., 1999), but did not deliver the same results. Treatments 1, 2 and 3 with osmium yielded the best images. In contrast, treatment 4, 5 and 6 with potassium permanganate provided images in which the sub-cellular structures are outlined less precisely, although, in treatment 6, osmium tetroxide, phosphotungstic acid and uranyl acetate were added. These observations correlate with those of other authors who also used potassium permanganate and osmium tetroxide (Hohmann-Marriot et al., 2005). The aforementioned comment that osmium tetroxide provides better fixation than potassium permanganate has also been observed in studies combining chemical fixation with freeze-substitution (Giddings, 2003). Based on the images obtained, the use of osmium tetroxide rather than potassium permanganate in BFSEM seems advisable.

The second criterion in the evaluation of the results was the measurement of the signal-to-noise ratio (SNR) (Thong et al., 2001; Sim et al., 2004). SNR is a parameter expressed in decibels (dB), which compares the signal collected (desired) with the level of background (noise) captured (undesired) of an image (Johnson, 2006). SNR values in SEM images depend on several factors such as the noise of the first electron beam, the

noise caused by fluctuations in the number of secondary electrons emitted when the primary beam hits the sample, and noise originating in the detector used. The noise due to the SE and BSE detector is insignificant compared to the others (Sim et al., 2004). Thus, it can be said that the value of SNR depends on the current of the electron beam, on the composition of the sample and on its topography (Sim et al., 2004). The values of SNR measured in this study varied, but reached values of almost 20 dB, which can be considered as a good SNR value. In treatments 1, 2, 3 and 5 the observation was made that, with the higher magnifications, the SNR value also increased, however not in a linear manner. This phenomenon could be related to the decrease of the visual field in the microscope with increased magnification, as diminution of the field is accompanied by a decrease in collected noise and consequently higher SNR values (Peters, 1985). An example of this was seen in treatment 2, in which SNR increased by more than 30% between 800X and 16000X. The lowest value of SNR was measured in treatment 4 with less than 10 dB at 16000X. In this case the potassium permanganate showed a low emission and a high noise, giving rise to somewhat blurred images. However, as the best images do not always correspond to the highest SNR values, visual estimation of the images is still of indisputable value.

It is possible to improve the BSE signal by using the so-called beam deceleration (BD) (Phifer et al., 2009). BD in an SEM allows improvements in both resolution and image contrast. The main feature of BD is that the sample is kept under a negative voltage current so that the primary electrons are stopped just before the sample surface is reached. Landing energy (LE) is the term that describes the energy of decelerated electrons when they impact with the sample. A recent study suggested that the greatest benefits could be obtained from BD when operating at low voltage (Ohta et al., 2012). However, as long as the landing energy (LE) does not exceed 5 kV, the results can be quite acceptable (Ohta et al., 2012).

The third criterion to evaluate the results of this study was microanalysis, or X-ray dispersive energy spectrometry, applied to the biological tissues processed for SEM according to the 6 treatments described. With this analytical technique a chemical characterization of the samples was performed by detecting the elements used for staining (contrast) them (Golstein et al., 2003). The spectra revealed the presence of the contrasting elements and gave information about their concentrations. Obviously, the tissue localization of these elements corresponds to the cellular and tissue structures to which they have affinity (Maunsbach and Afzelius, 1999).

Treatments 1, 2 and 3 produced varying concentrations of spectral peaks of osmium in the sample. In treatment 2 the concentration of osmium was almost 10% higher than in treatment 1, which, as already explained above, is undoubtedly due to HCT. However, in treatment 3 the osmium concentration was 40/45% lower than in the previous ones. In treatment 2, the samples were first treated with osmium according to Karnovsky, then with an intermediate step in TCH, followed by a simple osmium solution as already used in treatment 1. In this protocol, TCH functions as a ligand, which explains why the amount of osmium deposited is greater in this case. However, we have as yet no explanation as to why the osmium deposits were so low after treatment with osmium-potassium ferrocyanide. This is the case not only in comparison with treatment 2 but also with treatment 1, where a simple buffered solution of osmium tetroxide was used. It could be that after the application of Karnovsky's osmic solution, less osmium was quantitatively deposited, although judging from the TEM images, these deposits are very accurate in terms of cellular ultrastructure.

On the other hand, there were quite high deposits of uranyl acetate in treatment 3, which can be explained as follows: When a metal (uranyl acetate) is exposed to contact with the oxide of another metal (osmium tetroxide) the oxygen present reacts with the metal whose Gibbs free energy will be higher at room temperature (25ºC), spontaneously forming a bond between them. The Gibbs free energy variation of uranyl acetate ($\Delta G = -1031.8$ kJ /mol) is higher than that of osmium tetroxide ($\Delta G = -304.9$ kJ /mol), so that, in this case, the concentration of uranium present in the spectrum will be greater than that of osmium (Lide, 2005).

In treatment 4, manganese accumulated with relative concentrations ranging between approximately 14 and 45%. Treatment 5 is nothing other than treatment 4 with the additional step with uranyl acetate. The concentration of uranium in the sample is high, but that of manganese is approximately 33% lower than that found after treatment 4. This diminution might be caused by uranium.

A similar situation, but even more pronounced, is found in treatment 6, where the concentration of uranium is very high in the presence of osmium and manganese. The Gibbs free energy variation of potassium permanganate is $\Delta G = -737.6$ kJ/mol, so in treatment 5 the reduction of uranyl acetate compared to permanganate is energetically more favorable, which corresponds to the detected concentrations of uranium and manganese in the spectra (Lide, 2005).

Traditionally, it is believed that metals used for contrasting in electron microscopy become deposited in the samples independently of each other. The possible effects on the quantities deposited due to interactions, which take place between them during the staining process, is a quite new aspect.

Finally, a short comment on the fact that the pictures of the three organs examined reveal the characteristic ultra-structural features already visualized in conventional transmission electron microscopy (colon: Leeson, 1982; spinal ganglion: Andres, 1961; Pannese, 1969; anterior pituitary: see Bloom and Fawcett, 1975; exocrine pancreas:

Ekholm et al., 1962). Based on these findings, it seems appropriate to propose the application of the 2D BFSEM technique for the study of medical samples, as in the case of biopsies. Although electron microscopy (EM) does not find application in all areas of histo-pathological diagnosis, there are areas and situations in which EM can offer considerable benefits, which is also conceivable for BFSEM (Mestres, 2007).

ACKNOWLEDGEMENTS

REFERENCES

ANDRES KH (1961) Untersuchungen über den Feinbau von Spinalganglien. *Z Zellforsch,* 55:1-48.

BAJCSY P, LEE S-C, LIN A, FOLBERG R (2006) Three-dimensional volume reconstruction of extracellular matrix proteins in uveal melanoma from fluorescent confocal laser scanning microscope images. *J Microsc*, 221(Pt 1): 30-45.

BLOOM SE, GOODPASTURE C (1976) An improved technique for select silver staining of nucleolar organizer regions in human chromosomes. *Hum Genet,* 34: 199-206.

BLOOM W, FAWCETT DW (1975) A textbook of histology. WB Saunders Company, Philadelphia, London, Toronto.

BOZZOLA JJ, RUSSELL LD (1999) *Electron Microscopy Principles and Techniques for Biologists*. Jones and Bartlett Publishers, Sudbury, MA.

BRIGHTMAN MW, REESE TS (1969) Junctions between intimately apposed cell membranes in vertebrate brain. *J Cell Biol,* 40(3): 648-677.

BUSHBY AJ, P'NG KMY, YOUNG RD, PINALI CH, KNUPP C, QUANTOCK AJ (2011) Imaging three-dimensional tissue architectures by focused ion beam scanning electron microscopy. *Nature Protocols,* 6(6): 845-858.

CARTER HW (1980) Clinical applications of scanning electron microscopy (SEM) in North America with emphasis on SEM's role in comparative microscopy. *Scanning Electron Microscopy* 1980(3): 115-120. SEM Inc. AMF O'Hare (Chicago) IL (USA).

CREWE AV, LIN PS (1976) The use of backscattered electrons for imaging purposes in a scanning electron microscope. *Ultramicroscopy,* 1(3): 231-238.

DANILATOS GD (1988) Foundations of environmental scanning electron microscopy. *Avd Electron Electron Phys,* 71: 109-250.

DANILATOS GD (1994) Environmental scanning electron microscopy and microanalysis. *Mikrochim Acta,* 114/115: 143-155.

DEERINCK TJ, BUSHONG EA, LEV-RAM V, SHU X, TSIEN RY, ELISMAN MH (2010) Enhancing serial block-face scanning electron microscopy to enable high resolution 3-D nanohistology of cells and tissues. *Microsc Microanal*, 16(suppl. 2): 1138-1139.

DENK W, HORSTMANN H (2004) The serial block-face scanning electron microscopy to reconstruct three-dimensional tissue nanostructure. *PLoS Biol,* 2(11): e 329.

GEYER G (1969) Ultrahistochemie. Histochemische Arbeitsvorschriften für die Elektronenmikroskopie. Gustav Fischer Verlag, Stuttgart.

GIDDINGS TH (2003) Freeze-substitution protocols for improved visualization of membranes in high-pressure frozen samples. *J Microsc,* 212(Pt1): 53-61.

GLAUERT AM (1975) Fixation, dehydration and embedding of biological specimens. In: Glauert AM (ed). *Practical Methods in Electron Microscopy*. North-Holland Publishing Co. Amsterdam, Oxford and American Elsevier Publishing Co. Inc. New York.

GOLDSTEIN JI, NEWBURY DE, MICHAEL JR, RITCHIE NWM, SCOTT JHJ, JOY DC (2017) Scanning microscopy and X-Ray microanalysis. 4th edition. Springer, Heidelberg, New York.

HEGRE ES, BRASHEAR AD (1946) On visualizing the cut surface of tissue embedded in a paraffin block. *Anat Rec,* 94: 94.

HEGRE ES, BRASHEAR AD (1947) The block-surface method of staining as applied to the study of embryology. *Anat Rec,* 97(1): 21-28.

HEIMER L (1970) Bridging the gap between light and electron microscopy in the experimental tracing of fiber connections. In: Nauta WJH, Ebbesson SOE (eds). *Contemporary Research Methods in Neuroanatomy*. Springer-Verlag, Heidelberg, New York, pp 162-172.

HOHMANN-MARRIOT MF, BLANKENSHIP RE, ROBERSON RW (2005) The ultrastructure of *Chlorobium tepidum* chlorosomes revealed by electron microscopy. *Photosynthesis Res,* 86: 145-154.

JOHNSON DH (2006) Signal-noise ratio. *Scholarpedia,* 1(12): 2088. doi: 10.4249/scholarpedia.2088.

KNOTT G, ROSSET S, CANTONI M (2011) Focused ion beam milling and scanning electron microscopy of brain tissue. *J Vis Exp,* 53: e2588, doi: 10.3791/2588.

LAUE M, KIEFER G, LEIS B, PÜTZ N, MESTRES P (2005) Use of environmental scanning electron microscopy to study a resin block face. *Microscopy and Analysis,* 19(5): 17-19.

LEESON TS (1982) The terminal web of the duodenal enterocyte. *J Anat,* 134(4): 653-666.

LEIGHTON SB (1981) SEM images of block faces, cut by a miniature microtome within the SEM - A technical note. *Scanning Electron Microscopy*/ II, pp 73-76. SEM Inc., AMF O'Hare (Chicago) IL (USA).

LIDE DR (ed.) (2005) Handbook of Chemistry and Physics. Internet Version 2005 <http://hbcpnetbase.com> CRC Press, Boca Raton, FL (USA).

LUFT JH (1971) Ruthenium red and violet. I. Chemistry,

purification, methods of use for electron microscopy and mechanism of action. *Anat Rec,* 171: 347-368.

MALICK LE, WILSON RB, STETSON D (1975) Modified thiocarbohydrazide procedure for scanning electron microscopy: routine use for normal, pathological or experimental tissues. *Stain Technol,* 50(4): 265-269.

MAUNSBACH AB, AFZELIUS BA (1999) Biomedical Electron Microscopy. Illustrated Methods and Interpretations. Academic Press, San Diego, London, New York, Tokyo, Toronto.

MESTRES P, LOPEZ GOMEZ L, NUÑEZ LOPEZ T, DEL ROSARIO G, LUKAS SW, HARTMANN U (2014) The basement membrane of the isolated rat colonic mucosa. A light, electron and atomic force microscopy study. *Ann Anat,* 196(2-3): 108-118.

MESTRES P (2007) Applications of Electron Microscopy in Medicine. The State of the Art. MC 2007. *GIT Imaging and Microscopy,* 3/44-46.

MESTRES P, SCHÄFER KH, LINDEMANN B (1988) The epithelium of the taste bud of the frog. An investigation with backscattered electrons. *Beitr Elektronenmikroskop Direktabb Oberfl,* 21: 481-486.

MIKULA S, BINDING J, DENK W (2012) Staining and embedding the whole mouse brain for electron microscopy. *Nature Methods*, 9: 1198-1201. doi 10.1038/nmeth.2213.

OGURA K, HASEGAWA Y (1980) Application of backscattered electron image to biological specimens. *J Electron Microsc,* 29(1): 68-71.

OHTA K, SADAYAMA S, TOGO A, HIGASHI R, TANOUE R, NAKAMURA K-I (2012) Beam deceleration for block-face scanning electron microscopy of embedded biological tissue. *Micron,* 43: 612-620. doi: 10.1016/j.micron.2011.11.001.

PALADE GE (1952) A study of fixation for electron microscopy. *J Exp Med,* 95(3): 285-298.

PANNESE E (1969) Electron microscopical study of the development of the satellite cell sheath in spinal ganglia. *J Comp Neurol,* 135: 381-422.

PETERS KR (1985) Working at higher magnifications in scanning electron microscopy with secondary and backscattered electrons on metal coated biological specimens and imaging macromolecular cell membrane structures. *Scanning Electron Microscopy,* 1985 (Pt. 4): 1519-1544. SEM Inc., AMF O'Hare (Chicago) IL (USA).

PHIFER D, TUMA L, VYSTAVEL T, WANDROL P, YOUNG RJ (2009) Improving SEM imaging performance using beam deceleration. www.microscopy-today.com

PLATTNER H, ZINGSHEIM HP (1987) Elektronenmikroskopische Methodik in der Zell- und Molekularbiologie. Gustav Fischer Verlag, Stuttgart, New York.

PORTER KR, CLAUDE A, FULLAM EF (1945) A study of tissue culture cells by electron microscopy: Methods and preliminary observations. *J Exp Med,* 81(3): 233-246.

REYNOLDS EC (1963) The use of lead citrate at high pH as an electron-opaque staining for electron microscopy. *J Cell Biol,* 17: 208-212.

RICHARDSON KC, JARETT L, FINKE EH (1960) Embedding in epoxy resins for ultrathin sectioning in electron microscopy. *Stain Technol*, 35: 313-325.

SCHERTEL A, SNAIDERO N, HAN H-M, RUHWEDEL T, LAUE M, GRABENBAUER M, MÖBIUS W (2013) Cryo FIB-SEM: Volume imaging of cellular ultrastructure in native frozen specimens. *J Struct Biol,* 184(2): 355-360.

SEITER J, MULLER E, BLANK H, GEHRKE H, MARKO D, GERTHSEN D (2014) Backscattered electron SEM imaging of cells and determination of the information depth. *J Microsc,* 254 (2): 75-83.

SELIGMAN AM, WASSERKRUG HL, HANKER JS (1966) A new staining method (OTO) for enhancing contrast of lipid-containing membranes and droplets in osmium tetroxide fixed tissue with osmiophilic thiocarbohydrazide (TCH). *J Cell Biol,* 30(2): 424-432.

SIM KS, THONG JTL, PHANG JCH (2004) Effect of shot noise and secondary emission noise in scanning electron microscope images. *Scanning,* 26: 36-40.

THIÉBAUT F, RIGAUT JP, REITAN J, REITH A (1986) Spatial visualization of junctional complexes by backscattered electron imaging and silver staining, *Ultrastruct Pathol,* 10(3): 265-273.

THONG JTL, SIM KS, PHANG JCH (2001) Single-image signal-to-noise ratio estimation. *Scanning,* 23: 328-336.

TITZE B, DENK W (2013) Automated in-chamber specimen coating for serial block-face electron microscopy. *J Microscopy,* 250 (Pt. 2): 101-110.

TITZE B, GENOUD C (2016) Volume scanning electron microscopy for imaging biological ultrastructure. *Biol Cell,* 108(11): 307-323.

WANNINGER A (2007) The application of confocal microscopy and 3D imaging software in functional, evolutionary, and developmental Zoology: reconstructing myo- and neurogenesis in space and time. In: Méndez-Vilas A, Díaz J (eds). *Modern Research and Educational Topics in Microscopy.* Vol 1: 353-369. © Formatex 2007.